Journal of the European Ceramic Society 22 (2002) 2669–2675

www.elsevier.com/locate/jeurceramsoc

Fracture properties of SiC ceramics with oxynitride additives

Georg Rixecker[a,*], Koushik Biswas[a], Arno Rosinus[a], Siddharth Sharma[b], Ingo Wiedmann[a], Fritz Aldinger[a]

[a]*Max-Planck-Institut für Metallforschung and Institut für Nichtmetallische Anorganische Materialien der Universität Stuttgart, Pulvermetallurgisches Laboratorium, Heisenbergstraße 5, D-70569 Stuttgart, Germany*

[b]*Indian Institute of Technology, Kanpur 208016, India*

Received 24 October 2001; received in revised form 14 February 2002; accepted 6 March 2002

Abstract

Silicon carbide ceramics incorporating sintering additives from the system $AlN–Y_2O_3$ can be gas-pressure sintered to theoretical density. While commonly a combination of sesquioxides is used such as $Al_2O_3–Y_2O_3$, oxynitride additives offer the advantage that only a moderate nitrogen overpressure is required instead of a powder bed for thermochemical stabilization at the sintering temperature. In the present study aspects of the fracture behavior of these materials are addressed, namely the influence of anisotropic grain growth and processing flaws, additional toughening at high temperatures and thermal shock characteristics. They are correlated with microstructural data obtained by scanning electron microscopy.

Keywords: Ceramics; Fracture; Mechanical properties; Silicon carbide; Thermal shock

1. Introduction

Intense research activities have led to substantial progress in the properties of silicon carbide ceramics, with decisive steps being the invention of a solid state densification process with B and C sintering aids[1] and a liquid phase sintering route using Al_2O_3 and Y_2O_3 in combination.[2] Solid state sintered SiC materials (SSiC) generally offer the advantage of superior strength retention and creep resistance at high temperatures, because the highly covalent bonding character of the base material is conserved to a greater extent. For advanced structural applications requiring first and foremost high reliability, however, more favourable properties may be expected from liquid-phase sintered materials (LPS–SiC) because the liquid reduces the sintering temperature and allows homogeneous and fine-grained microstructures to be obtained. Starting from pure α-SiC or β-SiC powders, average grain sizes below 1 μm are achievable in fully dense ceramics.[3,4] If β-SiC powder containing a small amount of α-SiC seeds is utilized, the β-to-α phase transformation which proceeds during solution-reprecipitation sintering is accompanied by anisotropic grain growth.[5–7] This leads to platelet-reinforced microstructures, with grain sizes up to 5 μm, which exhibit enhanced fracture toughness due to the combination of the intergranular crack propagation mode—introduced by the presence of a glassy grain boundary phase—and energy dissipating processes in the crack wake.[8,9]

Oxides like SiO_2 and Al_2O_3, which are normally considered as thermodynamically stable, are prone to reactions with SiC at temperatures of about 2000 °C, leading to the formation of gaseous products such as CO, SiO and Al_2O.[10,11] In order to suppress these reactions, a powder bed is generally required. As an alternative, the additive system $AlN–Y_2O_3$ [11,12] was used where the decomposition of AlN into Al_l and N_2 can be efficiently controlled by using N_2 overpressure. Upon cooling, the melt solidifies and partly crystallizes to oxynitrides, the remaining amorphous phase forming a wetting film of about 1 nm [13] thickness between the SiC grains. The nitrogen content contributes to the refractoriness of the grain boundary phase by increasing its viscosity.[14] As already mentioned, the resistance against creep and oxidation is of outstanding importance for the performance of advanced structural ceramics. For the present rare earth oxynitride-densified LPS–SiC

* Corresponding author. Tel.: +49-711-6861-128; fax: +49-711-6861-138.

E-mail address: rixecker@mf.mpg.de (G. Rixecker).

0955-2219/02/$ - see front matter
PII: S0955-2219(02)00132-2

ceramics, which turn out to possess excellent creep and oxidation resistance, these issues will be discussed elsewhere.[15,16]

2. Experimental

A conventional powder technology process was followed for sample preparation. Appropriate mixtures of commercially available powders of α-SiC (HCST A10), β-SiC (HCST BF 12), AlN (HCST Grade C) and Y_2O_3 (HCST Grade C) were attrition milled in isopropanol, using polyamide vials and stirrers and Si_3N_4 milling media. After drying, the mixtures were granulated by sieving with a mesh width of 160 μm and cold isostatically pressed at 240 MPa. The green bodies were sintered in graphite-heated gas pressure furnaces (FCT, Germany) at temperatures up to 2050 °C and N_2 pressures up to 10 MPa. The sintering temperatures necessary for complete densification were found by increasing the temperature stepwise, so that the relative density determined by Archimedes' method was at least 99.3% after a dwell time of 1 h. Increasing the N_2 overpressure from 0.2 to 10 MPa after 0.5 h at the sintering temperature, i.e. after the porosity has closed, leads to higher strength values as a result of isostatic densification.[12] Further details of the preparation routine have been given elsewhere.[9]

The molar ratio of AlN to Y_2O_3 in the sintering additive was varied from 80AlN:20Y_2O_3 to 40AlN:60Y_2O_3 while maintaining a constant additive content of 10 or 7 vol.%. Samples with 20AlN:80Y_2O_3 showed poor wetting behavior of the liquid phase and are excluded from the further discussion. SiC mixtures with different contents of α-SiC and β-SiC were used, namely 100β, 96β:4α, 90β:10α, and 100α. To complete the phase transformation to α-SiC and to promote the evolution of a platelet-reinforced microstructure by anisotropic grain growth, sintered bodies containing β-SiC were subjected to heat treatments at 1950 °C under 0.2 MPa N_2 for times between 6 and 32 h.[9]

Specimen preparation for scanning electron microscopy (SEM) included a final polishing step with 1 μm diamond suspension prior to plasma etching in an equimolar mixture of CF_4 and O_2 (BioRad, Germany) to reveal the grain boundary phase. Microstructures were examined using either a conventional SEM (Cambridge Instruments, UK) or an instrument with thermal Schottky field emission cathode (Zeiss DSM 982, Germany), the acceleration voltage of which can be reduced to 3–5 keV while maintaining high resolution in order to avoid specimen charging. Grain sizes and aspect ratios were determined using an image analysis software (Imtronic, Germany).

Four-point bend strength testing was performed using fixtures with outer and inner spans of 40 and 20 mm, respectively. Samples with dimensions of 3×4×45 mm^3 were cut from larger sintered bars by means of a diamond saw. After grinding, the tensile surfaces were polished to a 3 μm finish and the tensile edges were bevelled. Room temperature testing was conducted with a servohydraulic test machine (Schenk, Germany) by loading the samples with a constant cross head speed of 5 mm/s. For each strength value, at least six measurements were averaged. Fracture toughness at ambient temperature was determined by the indentation crack length method. After polishing to a 1 μm finish, at least 10 Vickers indentations per specimen were introduced with a load of 100 N and loading times of 15 s. K_{Ic}^{ICL} was calculated from the lengths of edge cracks and indentation diagonals using a formula valid for semi-circular crack systems.[17] Young's moduli were measured by the pulse-echo method. For the K_{Ic} calculations, a value of 400 GPa was used throughout. High-temperature fracture toughness at crack tip temperatures between about 700 and 1060 °C was measured using the thermal stress method of Schneider et al.[18] This involves selective heating of the center of a notched disc (∅ 12×0.3 mm, surfaces polished to 1 μm finish) by means of a halogen reflector lamp in order to generate a temperature gradient. The temperature distribution across the disk is recorded using an optical pyrometer. The tangential stress field that is generated due to the temperature gradient causes crack initiation and growth at the notch root. After a short initial period (where a sharp starter crack is produced), the crack propagation is stable. The crack length during stationary heating is monitored by a long-distance microscope and recorded on videotape. From the thermally induced stress distribution, which can be derived analytically from the temperature field, K_{Ic}^{TS} is then calculated.[19] The indentation technique and the thermal stress technique were also utilized to introduce cracks for fractographic analysis at ambient and high temperature, respectively.

3. Results and discussion

3.1. Phase transformation and microstructural evolution

Using the CALPHAD method, phase diagram calculations in the AlN–Y_2O_3 system by Jeutter[20] predict a eutectic point at 60 mol% Y_2O_3. In contrast, sintering studies [9] show the lowest sintering temperature of LPS–SiC with AlN–Y_2O_3 additives to occur at 40 mol.% Y_2O_3. Residual yttria is also present down to an AlN:Y_2O_3 ratio of 60:40,[16] and the rate of transformation of β-SiC to α-SiC shows a maximum at that composition. For different materials with 10 vol.% of additives and a β-SiC:α-SiC ratio of 90:10 in the starting powder, the annealing times at 1950 °C after which either an α-SiC content of 90% or a fracture toughness

of $K_{Ic}^{ICL} = 5$ MPa$\sqrt{m}$ are reached, are plotted in Fig. 1 as a function of the AlN:Y_2O_3 ratio. These observations suggest that the eutectic point in the SiC-containing system is in the vicinity of 40 mol% Y_2O_3.

Apart from the composition dependence, the amount of phase transformation occurring during the first hour of sintering and the quickness of formation of the platelet microstructure increase with increasing volume fraction of the sintering aid and with increasing amount of α-SiC seeds. It has been argued that interfacial reactions rather than transport through the melt are rate-limiting for grain growth and microstructure development in the present LPS–SiC materials,[9] with nitrogen increasing the dissolution rate of SiC in the liquid phase. Since the overall kinetics is slow, grain growth is rather sluggish. Although the quantification of grain sizes in the SEM images is not straightforward due to the changing aspect ratio of the grains, the largest grain diameters observed range from 2 μm in as-sintered materials to 7 μm after annealing for up to 32 h at 1950 °C. Within the present range of compositions, plate-like grains with aspect ratios $\leqslant 4$ are obtained. Higher aspect ratios can be achieved by reducing the amount of α-SiC seeds[21] or by starting from ultrafine β-SiC and using a liquid phase with lower viscosity to reduce the annealing temperature.[4]

3.2. Fractography

During the evolution from globular to platelet microstructure, K_{Ic}^{ICL} gradually increases from 4.0±0.5 to 6.0±0.5 MPa$\sqrt{m}$ as energy dissipating processes in the crack wake become more efficient. In LPS–SiC, crack deflection, elastic bridging, mechanical interlocking and platelet fracture are commonly observed (Fig. 2), whereas pull-out of platelets is rarely encountered. Examples of the paths of cracks initiated by purely thermomechanical loading are shown in the SEM images of Fig. 3 (K_{Ic}^{TS} samples with a maximum crack tip temperature of 1060 °C, same material as in Fig. 2). Compared with the room temperature cracks, elastic bridging is much more extensive. In addition, platelet pull-out and viscous crack bridges are frequently observed, indicating the beginning of softening of the

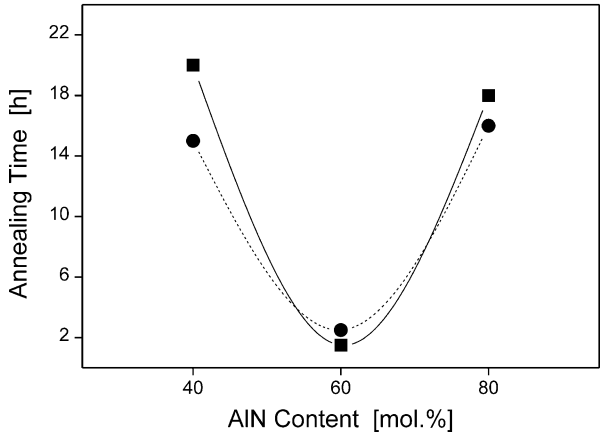

Fig. 1. Annealing times at 1950 °C that are necessary for reaching 90% α-SiC content (●) and $K_{Ic}^{ICL} = 5$ MPa m (■), respectively. Starting composition is 90β:10α-SiC, 10 vol.% additive content.

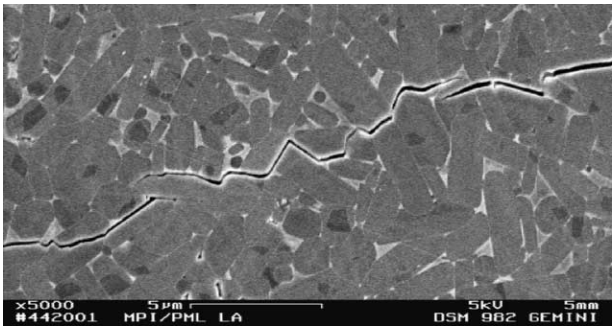

Fig. 2. Toughening mechanisms at room temperature in sample 90β:10α-SiC, 10 vol.% additive (60AlN:40Y_2O_3), post-sintering anneal for 16 h at 1950 °C.

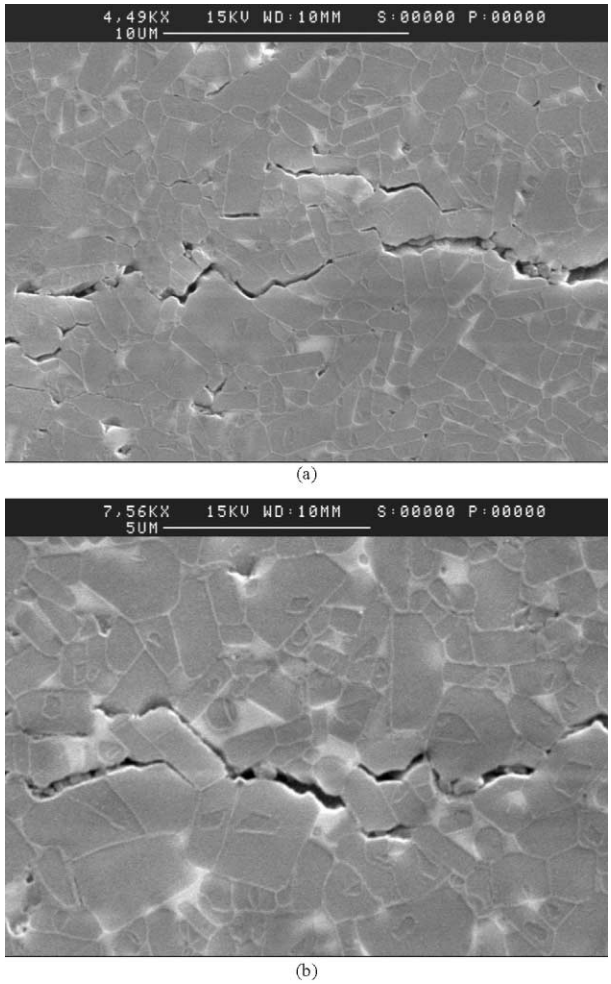

Fig. 3. Toughening mechanisms at crack tip temperatures up to 1060 °C in air, same material as in Fig. 2.

intergranular phase. This is reflected in a K_{Ic}^{TS} value of 7.5 ± 0.6 MPa$\sqrt{m}$, which is significantly higher than the room temperature value of $K_{Ic}^{ICL}=6.2\pm0.3$ MPa$\sqrt{m}$. It is interesting to note that in this material, the strength retention is still 100% at 1000 °C (and 87% at 1200 °C).[3] This means that the high-temperature fracture toughness is a quite sensitive indicator for the softening of the grain boundary phase.

Fig. 4 shows a plot of K_{Ic}^{ICL} versus σ_{4pt}^{RT} for various sample compositions. There appears to be a reciprocal relationship between the fracture toughness and the bending strength at room temperature—or, in other words, a correlation between the fracture strength and the grain size and/or shape distributions. For LPS–SiC materials with the present oxynitride additive system, the combined toughness and strength values can be improved, at a given composition, by subjecting the test specimens to an oxidation treatment (e.g. 0.2 h at 1200 or 1300 °C in air: broken curve in Fig. 4). For this oxidation-induced strengthening effect, different explanations are currently being considered, namely the creation of compressive stresses by selective oxidation of the intergranular oxynitrides[3] and/or the crystalline structure of the oxide films formed.[16] In both cases, surface and sub-surface flaws are effectively removed to a depth of tens of micrometers. Fractographic analysis frequently shows the fracture origins in samples which fractured under a high bending load ($\sigma_{4pt} > 600$ MPa) to be processing defects (pores) in the bulk of the material, in a zone which is not affected by the surface strengthening but still exposed to a high enough bending moment in 4-point geometry. The flaw size is generally in good agreement with the Griffith theory if one takes the average K_{Ic}^{ICL} of the material as fracture toughness. For example, Fig. 5 shows a flaw with a diameter of about 30 μm to be the fracture origin at $\sigma_{4pt}=650$ MPa and $K_{Ic}^{ICL}=5.5\pm0.5$ MPa$\sqrt{m}$.

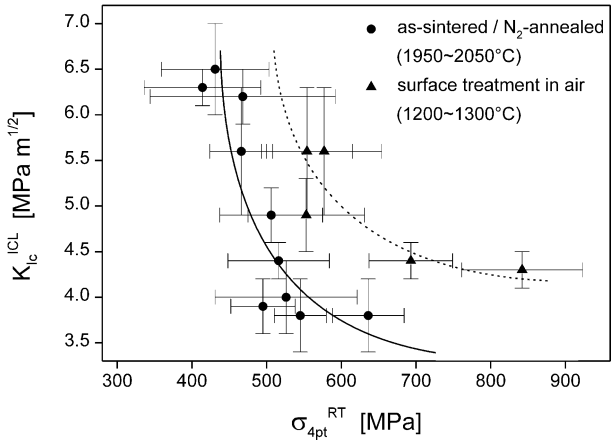

Fig. 4. Relationship between K_{Ic}^{ICL} and σ_{4pt}^{RT} for various LPS–SiC materials with oxynitride additives. Broken line: after surface oxidation for 0.2 h at 1200 to 1300 °C in air.

For grains without shape anisotropy, the fact that the fracture strength is correlated with both grain size and flaw size distributions has been discussed in-depth by Zimmermann and Rödel.[22] Essentially, the problem can be traced back to the question how the pair formed by a stress concentrator (a pore) and a potential microcrack origin (a large grain) responds to the applied stress to form the critical flaw. The basic conclusions drawn in [22] are expected to be equally valid in the present, anisotropic microstructures.

3.3. Thermal shock

In addition to the quasi-stationary K_{Ic}^{TS} test,[18] we performed standard thermal shock/retained strength testing [23] to reveal a possible dependance of the thermal shock tolerance on microstructural details. For this purpose, samples with identical chemical composition (10 vol.% additive, 60 AlN:40 Y_2O_3) but different microstructures were selected, as shown in Fig. 6—globular grains starting from pure 100α-SiC, partly developed platelets in as-sintered 90β:10α-SiC specimens, and fully developed platelet microstructure after annealing the 90β:10α-SiC material for 16 h at 1950 °C. They were heated to various temperatures (up to 700 °C in air, dwell time of 10 min) and quenched by dropping in water ($T_0=20$ °C) before measuring their 4-point bending strength. The σ_{4pt}^{RT} versus T curves show a sudden loss of strength at a critical temperature T_c, the critical temperature difference $T_S=T_c-T_0$ ranging from 350 K for the fine-grained globular microstructure to 500 K for the platelet microstructure. Fig. 7 presents the 'intermediate' case of as-sintered 90β:10α-SiC material.

A thermal stress parameter which can be interpreted as critical temperature difference, R_S, and a thermal stress damage resistance parameter, R_S^{IV}, can be estimated according to Hasselmann's model [23,24] by

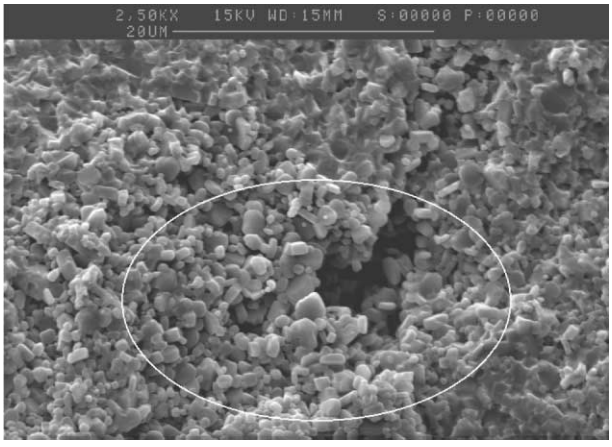

Fig. 5. Fracture origin of a specimen fractured at 650 MPa. The critical flaw is a pressing defect surrounded by a zone depleted in sintering additive (sample composition as in Fig. 2, post-sintering anneal for 7 h at 1950 °C, surface oxidized for 0.2 h at 1300 °C).

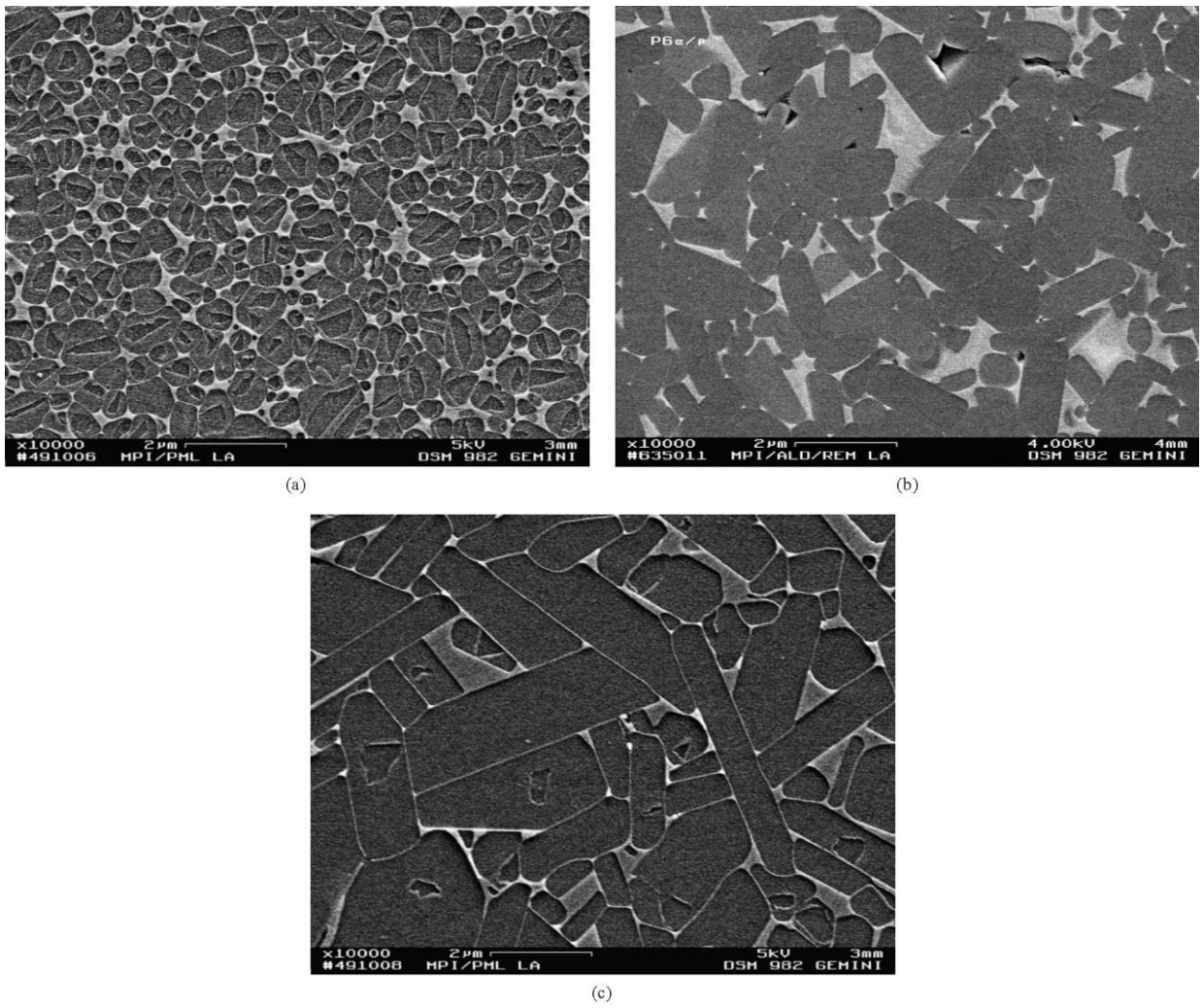

Fig. 6. Sample microstructures for thermal shock testing: (a) 100 α-SiC, as-sintered; (b) 90β:10α-SiC, as-sintered; (c) 90β:10α-SiC, annealed for 16 h at 1950 °C.

$$R_S = \sigma_c(1-\nu)/(\alpha E), \quad (1)$$

$$R_S^{IV} = (K_{Ic}/\sigma_c)^2. \quad (2)$$

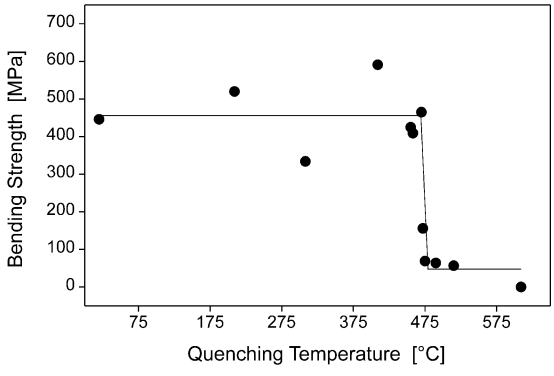

Fig. 7. Retained strength of the LPS–SiC ceramics according to Fig. 6(b) after quenching into water from the temperatures indicated.

Assuming E = 400 GPa, Poisson's ratio $\nu = 0.28$ and the thermal expansion coefficient $\alpha = 4.3 \times 10^{-6}$ K^{-1}, both quantities are listed in Table 1 together with the experimental strength and toughness data of the three materials. Due to the lower critical stress (fracture strength) values, σ_c, and higher Young's moduli, E, the threshold values R_S for crack initiation by thermal shock are lower in LPS–SiC than in monolithic silicon nitride ceramics [25] or Si_3N_4–SiC composites.[26] However, the hierarchy of the T_S values suggests that the thermal shock behavior is more likely to be governed by

Table 1
Thermal shock properties of the LPS–SiC ceramics from Fig. 6(a)–(c)

Microstructure	T_S [K]	R_S [K]	R_S^{IV} [10^{-4} m]	σ_{4pt}^{RT} [MPa]	K_{Ic}^{ICL} [MPa$\sqrt{m}$]
Globular	350	220	0.7	516±68	4.4±0.2
Platelet, as-sintered	455	210	1.1	506±69	4.9±0.3
Platelet, annealed	500	200	1.8	466±42	6.2±0.3

R_S^{IV} which gives a criterion for the resistance against crack propagation. In this picture, T_S is the temperature difference where the additional flaws generated by thermal shock become more severe than the flaws normally leading to failure during the strength test.[25]

4. Conclusions

1. LPS–SiC sintered with AlN–Y_2O_3 additives shows particularly rapid kinetics of phase transformation and microstructural evolution at a composition of AlN:Y_2O_3 = 60:40.
2. Due to an increasing efficiency of crack wake processes like elastic/viscous bridging and grain pull-out, the fracture toughness of platelet-reinforced microstructures is significantly enhanced at temperatures where softening of the grain boundary phase begins. At a composition of 80 AlN:20 Y_2O_3 and crack tip temperatures of about 1060 °C, a value of $K_{Ic}^{TS} = 8.0 \pm 0.5$ MPa$\sqrt{m}$ is reached.
3. Taking advantage of an oxidation-induced strengthening effect, the combined strength and toughness of oxynitride-sintered materials can be enhanced.
4. In high-strength materials, the critical flaws leading to fracture are processing defects in the bulk. Removal of these defects by improved powder conditioning and forming processes is expected to lead to materials with higher strength and reliability.
5. The thermal shock temperature is microstructure-dependant and reaches values of 500 K in platelet-strengthened microstructures.
6. The control of grain morphology that is possible by liquid phase sintering and post-sintering heat treatments gives an additional degree of freedom for tailoring mechanical properties.

Acknowledgements

The authors would like to thank Dr. Judy Schneider and Dr. André Zimmermann for fruitful discussions. We are also grateful to the technical staff of PML Stuttgart for assisting with the experimental work.

References

1. Prochazka, S., The role of boron and carbon in the sintering of silicon carbide. In *Special Ceramics,* (Vol. 6), ed. P. Popper. Br. Ceram. Res. Assoc., Stoke on Trent, 1975, pp. 171–181.
2. Omori, M. and Takei, H., Pressureless sintering of SiC. *J. Am. Ceram. Soc.*, 1982, **65**, C–92.
3. Rixecker, G., Wiedmann, I., Rosinus, A. and Aldinger, F., High-temperature effects in the fracture mechanical behaviour of silicon carbide liquid-phase sintered with AlN–Y_2O_3 additives. *J. Eur. Ceram. Soc.*, 2001, **21**, 1013–1019.
4. Kim, Y. W., Mitomo, M. and Hirotsuru, H., Grain growth and fracture toughness of fine-grained silicon carbide ceramics. *J. Am. Ceram. Soc.*, 1995, **78**, 3145–3148.
5. Lee, S. K. and Kim, C. H., Effects of α-SiC versus β-SiC starting powders on microstructure and fracture toughness of SiC sintered with Al_2O_3–Y_2O_3 additives. *J. Am. Ceram. Soc.*, 1994, **77**, 1655–1658.
6. Kodama, H. and Miyoshi, T., Fabrication and fracture behavior of novel SiC ceramics having rodlike grains. *J. Am. Ceram. Soc.*, 1992, **75**, 1558–1561.
7. Kim, Y. W., Mitomo, M., Emoto, H. and Lee, J. G., Effect of initial alpha-phase content on microstructure and mechanical properties of sintered silicon carbide. *J. Am. Ceram. Soc.*, 1998, **81**, 3136–3140.
8. Becher, P. F., Microstructural design of toughened ceramics. *J. Am. Ceram. Soc.*, 1991, **74**, 255–269.
9. Rixecker, G., Biswas, K., Wiedmann, I. and Aldinger, F., Liquid-phase sintered SiC ceramics with oxynitride additives. *J. Ceram. Process. Res.*, 2000, **1**, 12–19.
10. Mulla, M. A. and Krstic, D., Pressureless sintering of β-SiC with Al_2O_3 additions. *J. Mater. Sci.*, 1994, **29**, 934.
11. Nader, M., *Untersuchung der Kornwachstumsphänomene an flüssigphasengesinterten SiC-Keramiken und ihre Möglichkeiten zur Gefügeveränderung*. Doctoral thesis, University of Stuttgart, 1995.
12. Chia, K. Y., Boecker, W. D. G. and Storm, R. S., *Silicon Carbide Bodies Having High Toughness and Fracture Resistance and Method of Making Same*. US Patent 5,298,470, 1994.
13. Falk, L. K. L., Microstructural development during liquid phase sintering of silicon carbide ceramics. *J. Eur. Ceram. Soc.*, 1997, **17**, 983–994.
14. Hampshire, S., Nestor, E., Flynn, R., Besson, J.-L., Rouxel, T., Lemercier, H., Goursat, P., Sebai, M., Thompson, D. P. and Liddell, K., Yttrium oxynitride glasses: properties and potential for crystallisation to glass-ceramics. *J. Eur. Ceram. Soc.*, 1994, **14**, 261–273.
15. Biswas, K., Rixecker, G. and Aldinger, F., Mechanical properties of SiC-ceramics sintered with rare earth oxide additives. *J. Eur. Ceram. Soc.* (submitted for publication).
16. Schneider, J. A., Biswas, K., Rixecker, G. and Aldinger, F., Grain boundary phase evolution in liquid phase sintered silicon carbide during creep testing. *J. Am. Ceram. Soc.* (submitted for publication).
17. Anstis, G. R. P., Chantikul, P., Lawn, B. R. and Marshall, D. B., A critical evaluation of indentation techniques for measuring fracture toughness: I. direct crack measurements. *J. Am. Ceram. Soc.*, 1981, **64**, 533.
18. Schneider, G. A. and Petzow, G., Thermal shock testing of ceramics—a new testing method. *J. Am. Ceram. Soc.*, 1991, **74**, 98–102;
    Schneider, G. A., Magerl, F., Hahn, I. and Petzow, G., In-situ observations of unstable and stable crack propagation and R-curve behavior in thermally loaded disks. In *Thermal Shock and Thermal Fatigue Behaviour of Advanced Ceramics*, ed. G. A. Schneider and G. Petzow. Kluwer Academic, Dordrecht, 1993, pp. 229–244.
19. Gregory, R. D., The spinning circular disc with a radial edge crack: an exact solution. *Int. J. of Fracture*, 1989, **41**, 39.
20. Jeutter, A. *Untersuchung der Phasenbeziehungen im System Aluminiumnitrid-Yttriumoxid*. Diplom thesis, University of Stuttgart, 1993.

21. Keppeler, M., Reichert, H.-G., Broadley, J. M., Thurn, G., Wiedmann, I. and Aldinger, F., High temperature mechanical behaviour of liquid phase sintered silicon carbide. *J. Eur. Ceram. Soc*., 1998, **18**, 521–526.
22. Zimmermann, A. and Rödel, J., Generalized Orowan-Petch plot for brittle fracture. *J. Am. Ceram. Soc*., 1998, **81**, 2527–2532;
Zimmermann, A. and Rödel, J., Fracture statistics based on pore/grain-size interaction *J. Am. Ceram. Soc*. **82**, 1999, pp. 2279–2281.
23. Hasselmann, D. P. H., Elastic energy at fracture and surface energy as design criteria for thermal shock. *J. Am. Ceram. Soc*., 1963, **46**, 535.
24. Munz, D. and Fett, T., *Ceramics—Mechanical Properties, Failure Behaviour, Materials Selection*. Springer, Berlin, 1999.
25. Schneider, G. A. and Petzow, G., Thermal shock behaviour of Si_3N_4. *Key Eng. Mater*., 1994, **89–91**, 563–568.
26. Acchar, W., Gomes, U. U., Bressiani, A. H. and Bressiani, J. C., Study on thermal shock in Si_3N_4/SiC platelets. *J. Mater. Sci. Lett*., 1998, **17**, 2125–2127.